filter resulting when the gyro drifts, accelerometer errors, and DME biases are neglected performs nearly optimally. Hence, alignment can be accomplished by using an eighth-order filter when using one VOR/DME, or a seventh-order filter when using two DME's.

The quantitative results presented here are, of course, dependent upon the validity of the error models assumed. In particular, the VOR/DME error model proposed here has not been as thoroughly checked experimentally as the inertial navigation system model.

References

[1] Bryson, A. E., Jr. and Bobick, J. C., "Improved Navigation by Combining VOR/DME Information and Air Data," *Journal of Aircraft*, Vol. 9, No. 6, June 1972, pp. 420–426.

[2] Hemesath, N. B., "Optimal and Suboptimal Velocity-Aiding for VOR/DME Systems," *AIAA Journal*, Vol. 10, No. 1, Jan. 1972, pp. 24–30.

[3] Hemesath, N. B., Meyer, D. H., and Schweighofer, H. M., "Complementing VOR/DME with INS—An Improved Navigation System," Paper 690338, National Business Aircraft Meeting, Society of Automotive Engineers, Wichita, Kansas, March 26–28, 1969.

[4] Del Balzo, J. M., "Inertial Systems and Area Navigation in the U.S. Domestic Airspace," *Navigation*, Vol. 17, No. 4, Winter 1970–71, pp. 426–431.

[5] Holm, R. J., "Flight Evaluation of Inertial/DME/DME System," Rept. RD-70-24, May 1970, Federal Aviation Administration, Washington, D.C.

[6] Silver, M. and Greenberg, M., "Area Navigation—A Quantitative Evaluation of the Effectiveness of Inertial System Aiding," *Navigation*, Vol. 18, No. 4, Winter 1971–72, pp. 360–368.

[7] DeGroot, L. E. and Larsen, J., "Extended Capability from Existing Navaids," *Navigation*, Vol. 15, No. 4, Winter 1968–69, pp. 391–405.

[8] Pinson, J. C., "Inertial Guidance for Cruise Vehicles," *Guidance and Control of Aerospace Vehicles*, edited by C. T. Leondes, McGraw-Hill, New York, 1963, Chap. 4.

[9] Bobick, J. C. and Bryson, A. E., Jr., "Improved Navigation by Combining VOR/DME Information with Air or Inertial Data," SUDAAR 442, May 1972, Dept. of Aeronautics and Astronautics, Stanford University, Stanford, Calif.

[10] Erzberger, H., "Application of Kalman Filtering to Error Correction of Inertial Navigators," TN D-3874, Feb. 1967, NASA.

[11] Faurre, P., *Navigation Inertielle Optimale et Filtrage Statistique*, Dunod, Paris, 1971.

[12] Bryson, A. E., Jr. and Ho, Y. C., *Applied Optimal Control*, Xerox-Blaisdell, Waltham, Mass., 1969.

[13] Kalman, R. E., "A New Approach to Linear Filtering and Prediction Problems," *Transactions of the ASME, Ser. D: Journal of Basic Engineering*, Vol. 82, March 1960, pp. 35–45.

OCTOBER 1973 AIAA JOURNAL VOL. 11, NO. 10

Study of Vortex Rings Using a Laser Doppler Velocimeter

JOHN P. SULLIVAN,* SHEILA E. WIDNALL,† AND SHAOUL EZEKIEL‡
MIT, Cambridge, Mass.

Measurements of the axial and radial velocity distributions in vortex rings were made using a two-component laser Doppler velocimeter. The rings were generated by pulsing air through a sharp-edged orifice using a loudspeaker. The strength and vortex core size could be controlled somewhat by the duration and amplitude of the pulse. From detailed surveys of the velocity field, both the circulation and vorticity distribution were found for two different rings: one with a relatively thick core, the other with a thin core. The vorticity was found to be rather concentrated for both rings. Streamlines were also calculated and compared with observations. Vortex rings were found to be unstable to azimuthal perturbations; the observed mode number and growth rate are in reasonable agreement with theory.

Nomenclature

a = vortex core radius
n = number of unstable waves
r, z = coordinates
ρ, θ = polar coordinates, $r = r_0$
r_0 = vortex ring radius
U, V = velocities in r and z directions, respectively
U_0 = velocity of vortex ring
$\tilde{V} = \Gamma_0/4\pi r_0$
v_0 = swirl velocity in ρ, θ coordinates
Γ = circulation
Γ_0 = total circulation of vortex ring
ψ = streamfunction
ω = azimuthal component of vorticity
ω_0 = zero-order vorticity
ω_1 = first-order vorticity

Presented as Paper 73-105 at the AIAA 11th Aerospace Sciences Meeting, Washington, D.C., January 10–12, 1973; submitted January 19, 1973; revision received June 8, 1973. This work was supported by the Naval Air System Command (N0019-71-C-0220), the Air Force Office of Scientific Research (F44620-69-C-0090), and by the Joint Services Electronics Program (DAAB 07-71-C-0300).

Index category: Subsonic and Transonic Flow.

* Research Assistant, Department of Aeronautics and Astronautics, and Research Laboratory of Electronics.

† Associate Professor of Aeronautics and Astronautics. Member AIAA.

‡ Associate Professor of Aeronautics and Astronautics, and Research Laboratory of Electronics. Member AIAA.

Introduction

ALTHOUGH the fundamental interest in vortex rings has led to many flow visualization studies, there have been relatively few attempts to measure the detailed structure of the ring. This is due in part to the sensitivity of flows with concentrated vorticity to the insertion of a probe.

Tracer techniques were attempted by Krutzsch[1] in 1939 using aluminum flakes and Maxworthy[2] in 1970 using hydrogen bubbles, but due to strong axial gradients and associated radial velocities their results were inaccurate. Hot wire measurements[3] are hampered by probe interference and the difficulty of calibrat-

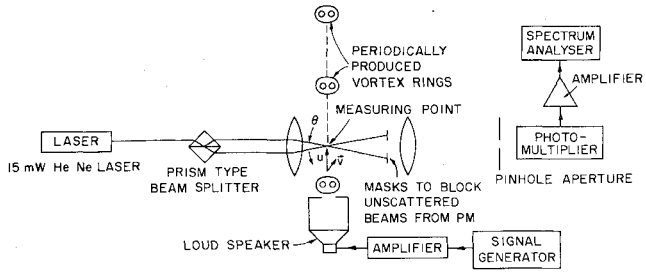

Fig. 1 One-dimensional dual scatter LDV system.

ing the probe in a flowfield where velocity is changing rapidly in magnitude and direction. These problems are circumvented in the present experiment by use of a laser doppler velocimeter (LDV).

Although the formation process is not well understood there are two models for steady vortex rings, the small core vortex where the ratio of core size to ring radius is small and Hill's spherical vortex where vorticity is distributed throughout a sphere. Several recent studies[4,5] of the motion of small core vortex rings give the translational velocity of the ring as[4]

$$U_0 = \Gamma_0/4\pi r_0[\ln 8r_0/a + A - 1/2] \quad (1)$$

where A is an integral over the tangential velocity distribution in the core (defined later). For solid-body rotation in the core, $A = \frac{1}{4}$ giving the classical Kelvin results. From the preceding equation the relevant nondimensional parameter to characterize the structure of the vortex core is

$$\tilde{V} = U_0/\Gamma_0/4\pi r_0 \quad (2)$$

Since the term in braces depends on the detailed distribution of vorticity it is of interest to measure this distribution. Also, models for studying the stability or entrainment will depend on the detailed structure of the ring. In the present study the circulation, streamlines and vorticity distribution are found throughout the ring from measurements of the axial and radial velocities made prior to instability.

Description of the Experiment

The experimental layout drawn with only a one-component LDV system for clarity is shown in Fig. 1. The LDV, which is a dual scatter system as described in Refs. 6 and 7, measures the Doppler shift of laser light scattered from particles in the flowfield. In the present experiment, the particles are 2.0 μ diameter oil particles generated by a standard mist lubricator normally used to lubricate high-speed bearings. It is estimated that the particles have a velocity which is within 0.5% of the fluid velocity.[8]

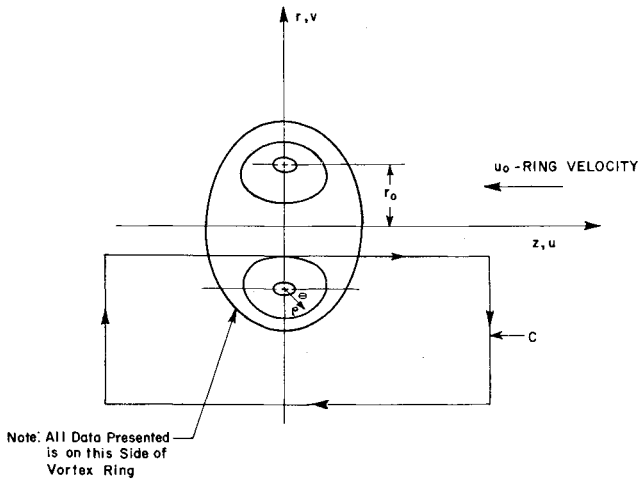

Fig. 2 Coordinate system for vortex ring data analysis.

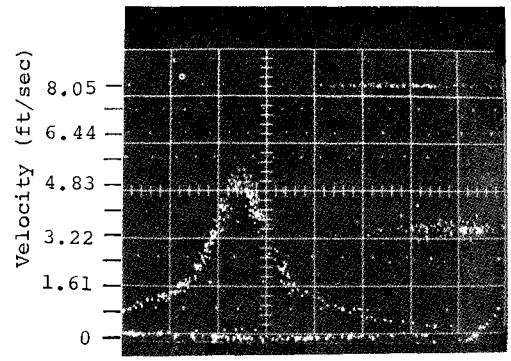

Fig. 3 U component of velocity at $r/r_0 = -0.876$ for ring 1. Time scale 20 msec/cm.

The actual two-dimensional system used is constructed by adding a second beam splitter (rotated 90° with respect to the first) to form four parallel beams in a diamond pattern. A more complete description of the experiment is given in Ref. 8.

Vortex rings are generated by pulsing air through a sharp-edged orifice using a loudspeaker—the circulation and core size are controlled by the amplitude and duration of the electrical signal applied to the loudspeaker.

The electronic system for processing the LDV signal is a data-sampling system that requires a periodic flowfield. To obtain a complete velocity profile, the rings are produced periodically; the distance between rings was approximately 100 ring radii to prevent any interaction between the rings.

The LDV system measures two components of velocity vs time at a fixed point in space as the vortex ring goes by the measuring point. The velocity distribution is transformed to the steady-coordinate system of Fig. 2 by letting $Z = U_0 t$ where U_0 is the instantaneous velocity of the vortex ring at the measuring point. This quasi-steady approximation assumes that the properties of the vortex ring do not change significantly (due to entrainment of surrounding fluid or wake shedding) in the time it takes the vortex ring to pass the measuring point. This is justified by flow visualization studies of the variation of ring speed U_0 and size of the ring.

Detailed surveys of a relatively thick core ring (denoted ring 1) and a thin core ring (ring 2) were made. Complete two-dimensional data were taken for ring 1 but only the component of velocity in the direction of ring travel was measured for ring 2.

Two samples of the velocity vs time data from ring 1 are shown in Figs. 3 and 4. There is a 180° ambiguity in the

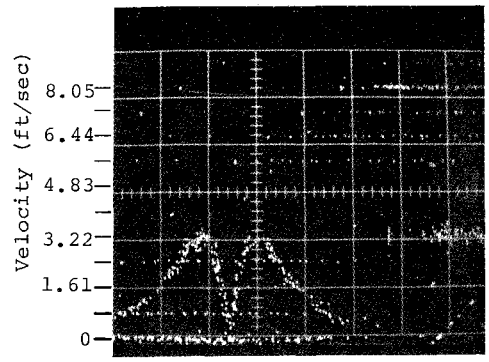

Fig. 4 V component of velocity at $r/r_0 = -1.08$ for ring 1. Time scale 20 msec/cm.

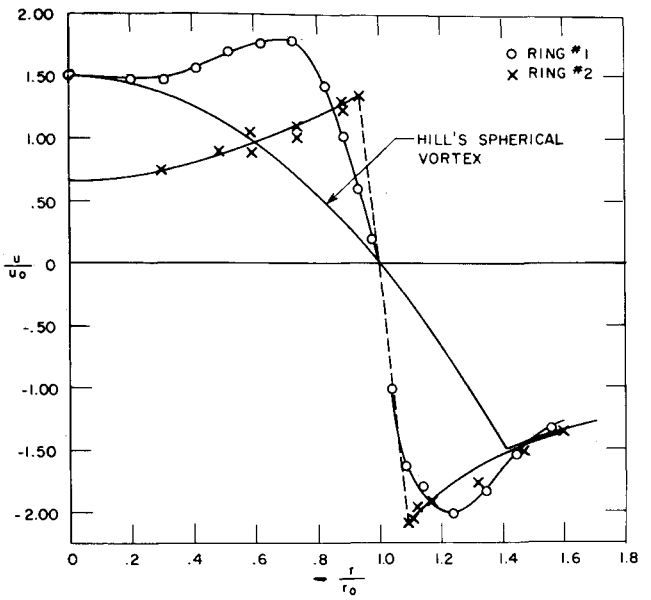

Fig. 5 U/u_0 vs r/r_0 along $z/r_0 = 0$.

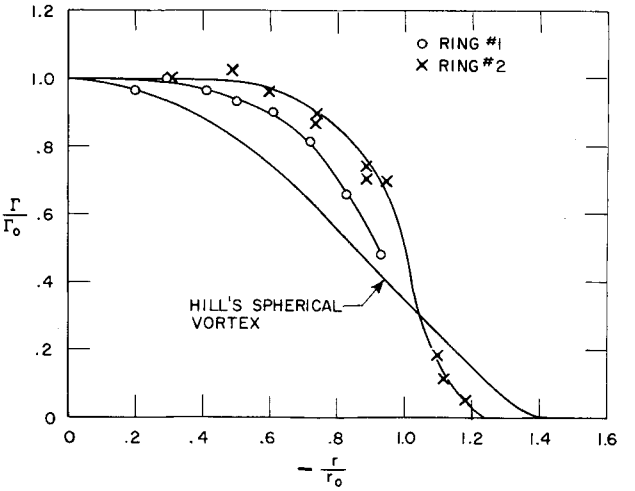

Fig. 6 Γ/Γ_0 vs r/r_0.

direction of velocity (since the detected frequency shift is always positive) which is easily resolved by flow visualization, indicating that the U component (Fig. 3) is always positive and the V component (Fig. 4) is negative to the left of the central zero and positive to the right. Data for ring 2 are similar, with velocities five times greater and the time scale five times faster since the ring speed U_0 of ring 2 is approximately five times that of ring 1.

Results and Discussion

The axial component of velocity U/U_0 vs r/r_0 along $z/r_0 = 0$ for the two vortex rings and Hill's spherical vortex for comparison is shown in Fig. 5. The value of r_0 is defined by the zero crossing of this curve and the core radius as one-half the distance between the positive and negative peak velocities. This gives a ratio of core radius to ring radius of $a/r_0 = 0.27$ for ring 1 and $a/r_0 = 0.075$ for ring 2, indicating that ring 2 is a relatively thin core ring while ring 1 has a relatively thick core but not nearly as thick as Hill's vortex where $a/r_0 = 1.414$. No data were taken in the core of ring 2 because of the lack of smoke particles in the vicinity of the core.

The circulation $\Gamma(r)$ is obtained by integrating the velocity along the curve C (Fig. 2); a rectangle with one side along r = constant and the other sides tending to infinity. Thus

$$\Gamma = \int_{-\infty}^{\infty} (U(z) - U_0)\, dz \tag{3}$$

In order to correct for the finite extent of the data it is assumed that $(U(z) - U_0) \sim 1/z^3$ after the last data point, which gives

$$\Gamma = \int_{z_1}^{z_2} (U(z) - U_0)\, dz + 1/2[U(z_2)z_2 - U(z_1)z_1] \tag{4}$$

where z_2 is the upstream cutoff and z_1 is the downstream cutoff.

The circulation was determined by finding the area under curves like Fig. 3 using a planimeter and adding the small correction from Eq. (4) due to the finite extent of the data. This correction was always less than 5%. The total circulation is the integral along $r = 0$. The resulting circulation distribution (Fig. 6) indicates again that ring 2 is the thinner core ring, with circulation more concentrated near $r/r_0 = 1.0$. The circulation calculated in this manner can give some indication of the vorticity distribution by differentiating the curves of Fig. 6. However, in order to obtain the vorticity, this derivative would have to be multiplied by an appropriate length corresponding to the distribution of vorticity in the Z direction. That is, the slope of the curves of Fig. 6 represents the vorticity weighted by an axial distribution length which is unknown. An alternate procedure will be used to determine the vorticity distribution.

A summary of the data is given in Table 1. A comparison between the actual value of $\tilde{V} = U_0/\Gamma_0/4\pi r_0$ and the value calculated for a small-core, solid-body rotation ring, $\ln 8r_0/a - \frac{1}{4}$, shows that the latter is 30–40% higher. This is due to the somewhat arbitrary definition of a and the fact that the core is not in solid-body rotation which implies A has a value other than $\frac{1}{4}$.

Since both components of velocity were measured on ring 1, the vorticity distribution throughout the vortex ring can be found. In order to minimize differentiation of data the fact that ω/r is constant on a streamline for a steady axisymmetric flow is utilized. The streamlines are found for the entire flowfield and the value of ω is calculated only along $z/r_0 = 0$ giving a value of ω on each streamline so ω is known everywhere.

Integration of velocity along convenient curves gives the streamfunction ψ so that the streamlines, lines of constant ψ, can be plotted. For an axisymmetric flow

$$d\psi = rU\, dr - rV\, dz$$

Integrating from $z = +\infty$ along a line r = constant gives

$$\psi(r = \text{const}, z) - \psi(r = \text{const}, \infty) = r\int_{-\infty}^{z} V(z')\, dz'$$

Assuming that $V \sim 1/z^3$ after some cutoff z_1 and nondimensionalizing

$$\frac{\psi(r,z)}{r_0^2 U_0} + \frac{1}{2}\left(\frac{r}{r_0}\right)^2 = \frac{r}{r_0}\left[\frac{V(z_1)z_1}{2U_0 r_0} - \int_{z_1}^{z} \frac{V(z'/r_0)}{U_0}\, d\left(\frac{z'}{r_0}\right)\right] \tag{5}$$

Table 1 Data summary

	r_0 (ft)	U_0 (ft/sec)	Γ_0 (ft²/sec)	a/r_0	$\tilde{V}^a$	$\ln 8r_0/a - 1/4$	$Re = \Gamma/\nu$
Ring 1	0.091	2.60	1.21	0.27	2.46	3.14	7780
Ring 2	0.111	13.5	6.07	0.075	3.10	4.42	37900

[a] Measured.

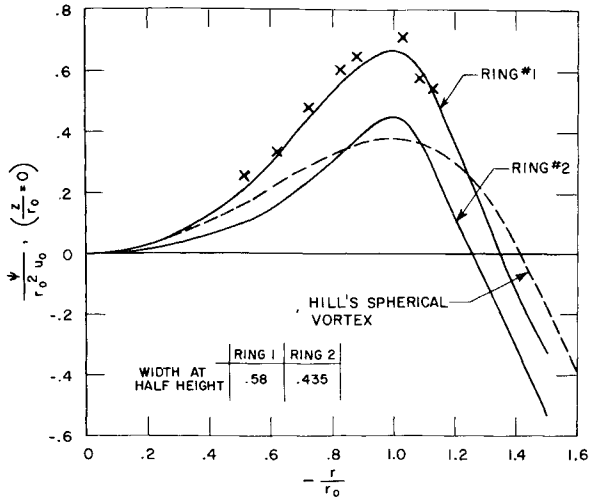

Fig. 7 $\psi/r_0^2U_0$ vs r/r_0 at $z/r_0 = 0$. × calculated from Eq. (5). Solid curves calculated from Eq. (6).

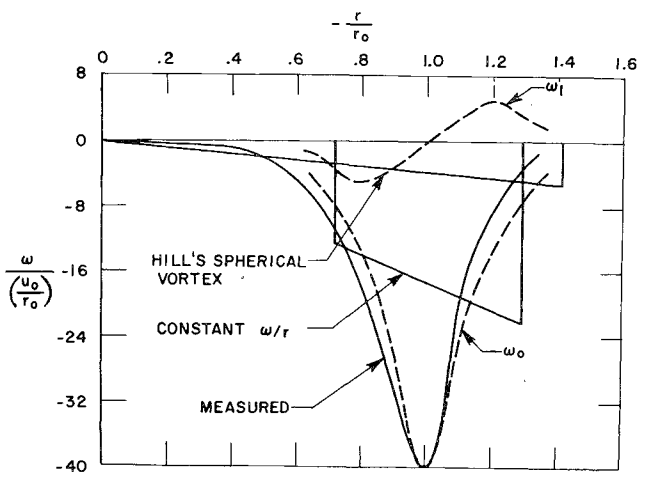

Fig. 9 Vorticity $\omega/(U_0/r_0)$ vs r/r_0 along $z/r_0 = 0$.

The streamfunction is thus determined by integrating curves like Fig. 4.

As a check, the streamfunction along $z/r_0 = 0$ is calculated by integrating the U component of velocity in Fig. 5 using

$$\frac{\psi(r,0)}{r_0^2U_0} = \int_0^{r/r_0} \left(\frac{r'}{r_0}\right) \frac{U(r'/r_0)}{U_0}\, d\left(\frac{r'}{r_0}\right) \tag{6}$$

The values of ψ along $z/r_0 = 0$ from the two methods are shown in Fig. 7. This critical check of calculating ψ from different data sets indicates that the over-all consistency of the data is very good. The actual streamlines are shown superposed on a strobe photograph of ring 1 in Fig. 8.

The vorticity ω is calculated along $z = 0$ differentiating the data

$$\frac{\omega(r,0)}{(U_0/r_0)} = \left.\frac{\partial(V/U_0)}{\partial(z/r_0)}\right|_{z=0} - \left.\frac{\partial(U/U_0)}{\partial(r/r_0)}\right|_{z=0}$$

The first term is the slope of the curves of Fig. 4 at $z = 0$ and the second term is obtained by differentiating the smoothed curve of Fig. 5. The results of differentiating the first term show scatter in the immediate vicinity of $r/r_0 = 1$ caused in part by the directional ambiguity of the LDV system. The V component of velocity rapidly changes from a large positive value to a large negative value giving data curves (Fig. 4) in which the determination of the slope at $z = 0$ is difficult. The vorticity distribution along $z = 0$ (Fig. 9) shows the expected concentration of vorticity in the core.

Using the fact that ω/r is constant on streamlines in conjunction with Figs. 8 and 9, the vorticity at any point in the ring can be found. It is estimated that roughly 85% of the vorticity is within the $\psi/r_0^2U_0 = 0.4$ streamline.

From the circulation distribution (Fig. 6) it is expected that ring 2 would have an even more concentrated vorticity distribution. These results on the concentration of vorticity are in contrast to the experimental results presented by Maxworthy.[2] He used a hydrogen bubble technique to measure the velocity distribution within a vortex ring and concluded that the vorticity is more spread out. His experiments, however, were carried out at much lower Reynolds numbers where the vorticity is probably more diffuse.

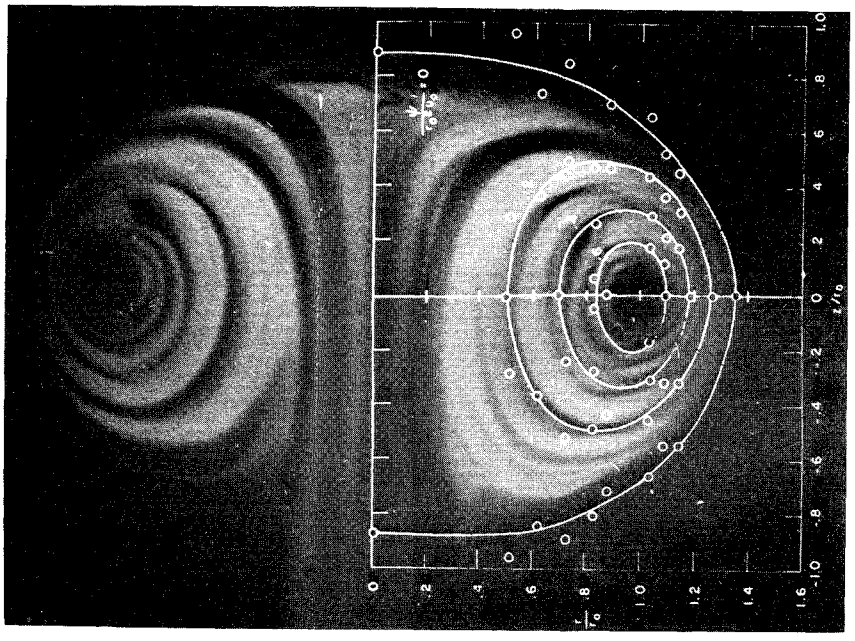

Fig. 8 Side view of ring 1 with measured streamline superposed.

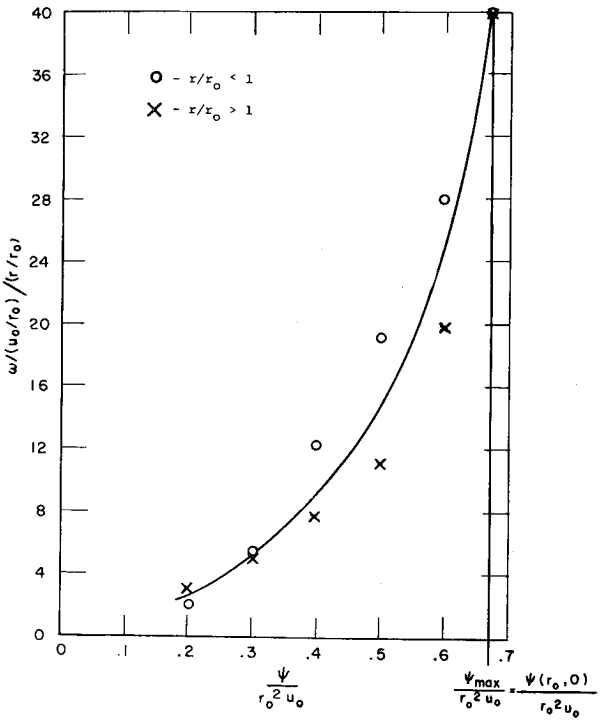

Fig. 10 Nondimensional ω/r vs ψ.

Figure 9 also shows the vorticity distribution for a small-core solid-body rotation ring (using the measured value of a/r_0) and Hill's spherical vortex. This comparison shows that for rings of the same size and velocity of translation neither model properly describes the experimentally produced vortex rings.

In a steady axisymmetric flow $\omega/r = F(\psi)$. Most theories assume $F(\psi)$ is a constant, but Fig. 10 shows that this is not the case.

Ring Properties from Vorticity Measurements

From the measured vorticity distribution along $z/r_0 = 0$, we can calculate the circulation and the velocity parameter $\tilde{V}$ by using the theory presented by Bliss.[4] In this work, the solution for the vorticity distribution within a slightly curved vortex filament was obtained by the method of matched asymptotic expansions. This theory shows that the vorticity distribution in a slightly curved filament may be written

$$\omega(\rho) = \omega_0(\rho) + (a/r_0)\omega_1(\rho)\sin\theta$$

where ω_0 is the vorticity distributed in a straight filament with radial symmetry and ω_1 is the small perturbation due to curvature. ω_0 is symmetric about $r = r_0$ ($\rho = 0$) and ω_1 is antisymmetric. We may use these properties to obtain ω_0 directly from the measured data since ω_0 is then the average value of the measured vorticity for points equally spaced about $r/r_0 = 1$.

If ω_0 is known for a vortex ring, the circulation and ring velocity can be calculated. The functions ω_0 and ω_1 are shown in Fig. 9.

The circulation of the ring in terms of ω_0 is just

$$\Gamma_0 = 2\pi \int_0^\infty \left(\frac{\rho}{r_0}\right)\left[\frac{\omega_0}{U_0/r_0}\right]\frac{d\rho}{r_0}[U_0 r_0]$$

Direct numerical integration of ω_0 calculated from the measured vorticity ω gives a value for Γ_0 of 1.17 ft^2/sec in close agreement with the measured value 1.21 ft^2/sec (Table 1).

The nondimensional ring velocity $\tilde{V}$ can also be determined from the measured vorticity. The nondimensional self-induced velocity of a vortex ring with an arbitrary distribution of vorticity is given by

$$\tilde{V} = \ln(8r_0/a) + A - \tfrac{1}{2} = \ln 8 - \tfrac{1}{2} + (A - \ln a/r_0)$$

where

$$A = \lim_{\bar{\rho}\to\infty}\int_0^\infty \hat{v}_0{}^2(\bar{\rho}')\bar{\rho}'\,d\bar{\rho}' - \ln\bar{\rho}$$

$\hat{v}_0$ is the nondimensional swirl velocity (in ρ, θ coordinate system) $\hat{v}_0 = v_0 2\pi a/\Gamma_0$ and $\bar{\rho} = \rho a/r_0$ where a is some typical dimension in the vortex core. (Actually, the parameter $A - \ln a/r_0$ is independent of the choice of length scale.)

Straightforward manipulation yields a formula for the group $A - \ln a/r_0$ in terms of the zeroth-order vorticity ω_0. The results are

$$A - \ln\frac{a}{r_0} = \frac{-2\displaystyle\int_0^\infty \bar{\rho}\omega_0(\bar{\rho})\ln\bar{\rho}\int_0^{\bar{\rho}}\bar{\rho}'\omega_0(\bar{\rho}')\,d\bar{\rho}'\,d\bar{\rho}}{\left[\displaystyle\int_0^\infty \bar{\rho}\omega_0(\bar{\rho})\,d\bar{\rho}\right]^2}$$

If the vorticity is uniform within a radius $r = a$, this expression gives the familiar result $A = \frac{1}{4}$. Direct numerical integration of this formula using the values of ω_0 obtained from the measured vorticity gives $\tilde{V} = 3.01$ as compared with a measured value of 2.46, an error of 20%. This is in somewhat better agreement than the value 3.14 obtained by assuming uniform vorticity. Since the ratio of core size to radius is 0.27 perhaps a 20% discrepancy between experiment and an asymptotic theory which assumes $a/R \ll 1$ is not surprising.

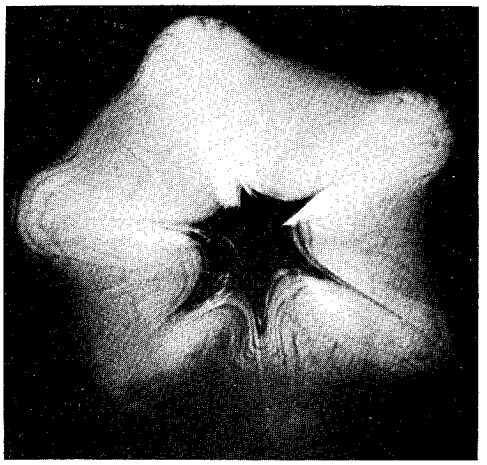

Fig. 11 Flow visualization of the vortex ring instability; $n = 6$.

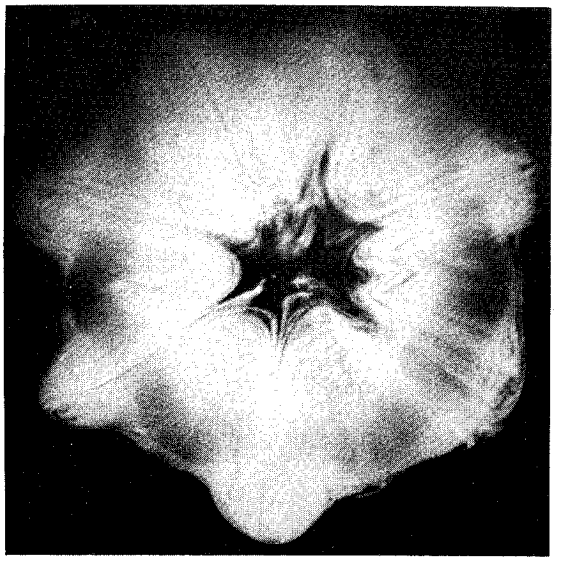

Fig. 12 Flow visualization of the vortex ring instability; $n = 7$.

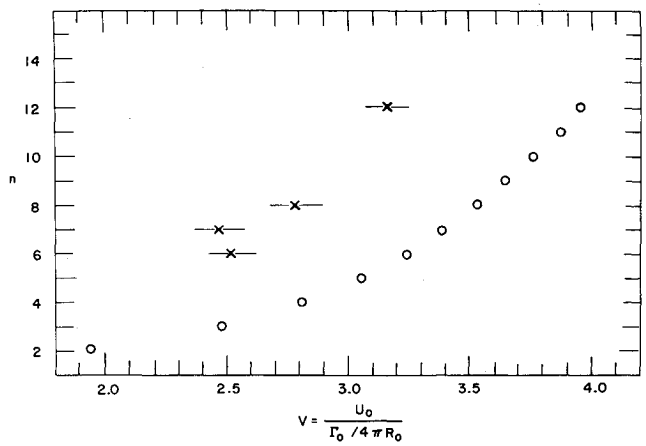

Fig. 13 Number of waves in the unstable mode as a function of $\tilde{V} = U_0/(\Gamma/4\pi R)$. × = experiment. ○ = theoretical prediction at maximum amplification.

A value of $A = 0.136$ is obtained when $a/r_0 = 0.27$ as defined in Fig. 5.

Stability

The problem of the stability of vortex rings was treated in a separate study[9] which concluded that vortex rings in an ideal fluid are unstable to azimuthal perturbations. Since these instabilities were always observed in our experiments, the measurements of the structure of the ring were made upstream of the development of the instability. The measurements of the structure of the core also provided some necessary information to compare the experiments with theory. Front-view photographs of an $n = 6$ and $n = 7$ mode instability are shown in Figs. 11 and 12. The actual observed mode number n of the instability is shown in Fig. 13 as a function of $\tilde{V} = U_0/\Gamma_0/4\pi R_0$. Also shown is the value of n that is predicted to be the most unstable for that value of $\tilde{V}$. Although the trend of increasing n with increasing $\tilde{V}$ (decreasing core size) is in agreement with the theoretical predictions, the actual values of n vs $\tilde{V}$ are not in good agreement. This is probably because the ratio of wavelength to vortex core radius of the unstable mode is not small as required by the asymptotic theory. For example, theory predicts that the $n = 6$ mode should be unstable for $\tilde{V}$ of approximately 3.2. For the observed instability, the value of $\tilde{V}$ obtained from the measured circulation was 2.5 while $\tilde{V}$ obtained from the measured vorticity distribution is 3, in much better agreement with the theoretical predictions. The measured radial perturbation of the ring because of the instability as a function of time is shown in Fig. 14. The growth of the perturbation during the early stages of the instability shows good agreement with the theoretical predictions. This is due in part to the fact that the amplification rate for an unstable mode is insensitive to both $\tilde{V}$ and modal number n.

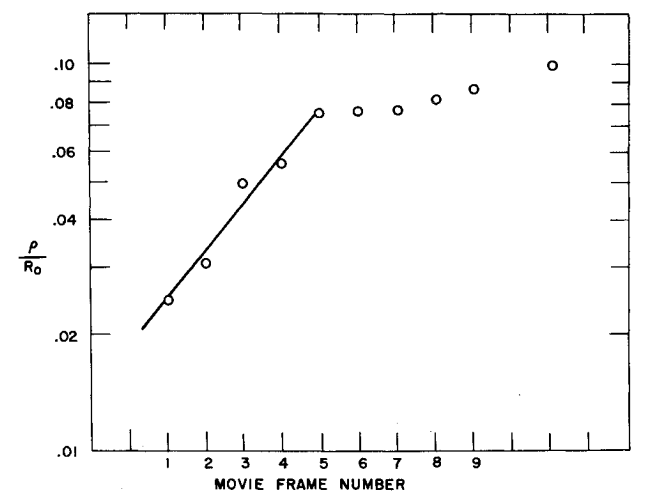

Fig. 14 Percent radial perturbation for the vortex ring of Fig. 12 measured at each strobe movie frame (time between frames 14.5 msec); exponential growth $\alpha_x = 0.69$; theoretical prediction $\alpha_x = 64$.

References

[1] Krutzsch, C. H., "Über eine experimentell beobachtete Erscheining an Werbelringen bei ehrer translatorischen Beivegung in Werklechin," *Flussigheiter Annalen der Physik*, Vol. 5, Folge Band 35, 1939, pp. 497–523.

[2] Maxworthy, T., "The Structure and Stability of Vortex Rings," *Journal of Fluid Mechanics*, Vol. 51, No. 1, 1972, p. 15.

[3] Johnson, G. M., "Researches on the Propagation and Decay of Vortex Rings," ARL TR 70-0093, June 1970, Aerospace Research Labs., Wright-Patterson Air Force Base, Ohio.

[4] Widnall, S. E., Bliss, D. B. and Zalay, A., "Theoretical and Experimental Study of the Stability of a Vortex Pair," *Proceedings of the Symposium on Aircraft Wake Turbulence*, Plenum Press, 1971.

[5] Fraenkel, L. E., "Examples of Steady Vortex Rings of Small Cross-section in an Ideal Fluid," *Journal of Fluid Mechanics*, Vol. 51, No. 1, 1972, p. 119.

[6] Rudd, M. J., "A New Theoretical Model for the Laser Dopplermeter," *Journal of Scientific Instruments* (*Journal of Physics E*), Ser. 2, Vol. 2, pp. 55–58.

[7] Lennert, A. E., Brayton, E. B., and Crosswy, F. L., "Summary Report of the Development of a Laser Doppler Velocimeter to be Used in AEDC Wind Tunnels," TR 70-101, 1970, Arnold Engineering Development Center, Arnold Air Force Station, Tenn.

[8] Sullivan, J. P., "Experimental Investigation of Vortex Rings and Helicopter Rotor Wakes Using a Laser Doppler Velocimeter," Ph.D. thesis, Feb. 1973, Dept. of Aeronautics and Astronautics, MIT, Cambridge, Mass.

[9] Widnall, S. E. and Sullivan, J. P., "On the Stability of Vortex Rings," *Proceedings of the Royal Society* (*London*), *Ser. A*, Vol. 332, 1973, pp. 335–353.